Ocean Modelling 134 (2019) 42–50

Contents lists available at ScienceDirect

Ocean Modelling

journal homepage: www.elsevier.com/locate/ocemod

TVDal: Total variation diminishing scheme with alternating limiters to balance numerical compression and diffusion

Lei Lin[a,b], Zhe Liu[b,1,*]

[a] State Key Laboratory of Estuarine and Coastal Research, East China Normal University, Shanghai 200062, China
[b] Key Laboratory of Marine Environment and Ecology (Ocean University of China), Ministry of Education, Qingdao 266100, China

ARTICLE INFO

Keywords:
Advection schemes
TVDal
Compression
Diffusion

ABSTRACT

Total variation diminishing (TVD) advection schemes are widely used in ocean modelling. Due to the constraints of flux limiters, TVD schemes with common single flux limiters of second-order or third-order accuracy exhibit defects associated with numerical compression or diffusion. To reduce the numerical errors induced by these numerical defects, a TVD method employing alternating flux limiters (TVDal) is proposed. The principle of TVDal is to alternately use a compressive and a diffusive limiter in different time steps. Through balancing the compression of the Superbee limiter and the diffusion of other flux limiters, a reduction of ~60% of numerical errors in one-dimensional benchmark tests can be achieved with the TVDal scheme. In addition, the TVDal scheme combined with the Strang-splitting method is proposed for multi-dimensional advection. For an idealized 2D experiment with oblique advection, the Strang-splitting TVDal scheme features good shape retention with much lower numerical errors. The TVDal scheme has also been applied to model tidally induced internal lee waves, indicating that TVDal has the potential ability to balance the numerical compression and diffusion of conventional TVD schemes for cases with highly nonlinear, stratified, and nonhomogeneous flow fields. Finally, the principles of the TVDal scheme also show the potential application to conventional high-order TVD schemes.

1. Introduction

Advection is a common physical process that plays an important role in ocean modelling. The choice of advection schemes has a significant influence on the simulation of ocean dynamics and mass transport (e.g., Bernard et al., 2006; Gerdes et al., 1991; Hecht et al., 1998; Lévy et al., 2001; Liu and Xue, 2009; Mohammadi-Aragh et al., 2015; Sommer et al., 2009; Winther et al., 2007). It is of wide interest to find an accurate and non-costly scheme for ocean modelling.

Traditional low-order advection schemes such as the first-order upwind scheme have excessive numerical diffusion (e.g., Pietrzak, 1998). High-order advection schemes such as the central difference scheme (CDS) significantly alleviate numerical diffusion but introduce spurious oscillations and even induce nonlinear instability (Yang and Przekwas, 1992). CDS dispersion results lead to undershooting or overshooting consequences (e.g., Yang and Przekwas, 1992; Pietrzak, 1998; Zhang et al., 2015). Therefore, CDS is usually used in conjunction with explicitly increased dissipation. Several methods are used to eliminate the numerical oscillations, e.g., the flux-corrected transport (FCT) scheme (Boris and Book, 1973; Zalesak, 1979), the (weighted) essentially non-oscillatory (ENO/WENO) scheme (e.g., Harten et al., 1987; Shi et al., 2002), and the total variation diminishing (TVD) scheme (Harten, 1983).

Among the schemes mentioned above, TVD uses flux limiters to preserve monotonicity and avert spurious oscillations (Harten, 1983). Given a variable c, the total variation (TV) in a discrete solution is defined as

$$TV(c^n) = \sum_{i=1}^{N} |c_{i+1}^n - c_i^n|, \tag{1}$$

where the superscript n and subscript i denote the number of time steps and space nodes, respectively, and N is the total number of nodes. The TVD constraints are satisfied if

$$TV(c^{n+1}) \le TV(c^n). \tag{2}$$

Different flux limiters have produced different TVD schemes which are widely used in ocean models. Pietrzak (1998) added the Van-Leer (or Harmonic), Monotonic Upstream-Centered Scheme for Conservation Laws (MUSCL), Minmod, and Superbee schemes to the Princeton Ocean Model (POM), which resulted in better modeling results for

* Corresponding author.
E-mail address: zliu@ouc.edu.cn (Z. Liu).
[1] Present address: Department of Earth Sciences, National Natural Science Foundation of China.

https://doi.org/10.1016/j.ocemod.2019.01.002
Received 25 September 2018; Received in revised form 26 December 2018; Accepted 6 January 2019
Available online 07 January 2019
1463-5003/

Table 1
Several types of typical Sweby's TVD schemes and their flux-limiters.

Names	Flux-limiters $\psi(r)$	Compressive/Diffusive	References
Superbee	$\psi(r) = \max[0, \min(2r, 1), \min(r, 2)]$	Compressive	(Roe, 1985)
Van-Leer (or Harmonic)	$\psi(r) = (r + \lvert r\rvert)/(r + 1)$	Diffusive	(Van Leer, 1974; Van Leer, 1977)
Minmod	$\psi(r) = \max[0, \min(r, 1)]$	Diffusive	(Roe, 1985)
MUSCL	$\psi(r) = \max[0, \min(2r, \frac{r+1}{2}, 2)]$	Diffusive	(Van Leer, 1974; Zalesak, 1987)
HSIMT	$\psi(r) = \max[0, \min(2r, 2, \beta)]$ $\beta = (-\frac{1}{4}\kappa + \frac{1}{2} + \frac{1}{12}\frac{1}{\kappa})r + (\frac{1}{4}\kappa + \frac{1}{2} - \frac{1}{12}\frac{1}{\kappa})$ and $\kappa = 1 - \lvert u\Delta t/\Delta x\rvert$	Diffusive	(Wu and Zhu, 2010)

temperature and salinity than those of the traditional central differencing scheme. The Superbee scheme has also been used in dispersive surface and internal wave modeling (e.g., Shi et al., 2015; Liu et al., 2016). Mercier and Delhez (2010a; 2010b) modified the Superbee scheme for the depth-integrated transport equation and additional variables with consideration of their sum in ocean modelling. Shi et al. (2012) implemented the MUSCL constraints into a Boussinesq model to address breaking waves and coastal inundation. Wu and Zhu (2010) developed a new spatial third-order HSIMT (High-order Spatial Interpolation at the Middle Temporal level) scheme with a Swebyem TVD limiter and applied it to study the Changjiang River plume (Wu, 2015; Wu et al., 2011).

However, these frequently used TVD schemes are either compressive (anti-diffusive) or diffusive, depending on the limiters used. For example, the Superbee scheme is compressive, whereas the other aforementioned TVD schemes are diffusive (e.g., Jeng and Payne, 1995; Yang and Przekwas, 1992; Wu and Zhu, 2010; Naughten et al., 2017). Fringer et al. (2005) simulated internal waves using several different TVD schemes in a completely closed domain, e.g., a lake, where the background potential energy (BPE) was conserved. Hence, in idealized configurations, the BPE represents an indicator that can indicate how and to what extent simulated energy departs from initial PE. If PE increases/decreases, the authors adopted diffusion/compression-type TVD schemes to counteract the changes in PE. However, in practice, it is difficult to propose a universally valid indicator function for ocean modelling due to the changes to BPE caused by physical mixing.

In this study, TVD with the alternating application of a dissuasive and compressive limiter (TVDal) is proposed to balance the numerical diffusion and compression issues. This paper is organized as follows. Section 2 introduces the TVDal scheme. The TVDal scheme is tested using one-dimensional (1D) and two-dimensional (2D) benchmark experiments in Section 3. In Section 4, the TVDal scheme is applied to non-hydrostatic ocean modelling, i.e., a tidally induced internal lee wave. The ratios of combined limiters, issues related to higher-order schemes, and the problem of local extrema are then discussed in Section 5. Finally, a brief conclusion is given in Section 6.

2. TVD scheme and the alternating limiter

2.1. TVD scheme and flux limiters

Consider the 1D linear advection equation

$$\frac{\partial c}{\partial t} + u\frac{\partial c}{\partial x} = 0, \tag{3}$$

where t is the time, x is the spatial coordinate, and $c = c(x, t)$ is the variable advected by the constant advection speed u. Eq. (3) can be discretized in the C-grid as follows:

$$c_i^{n+1} = c_i^n - \lambda(\hat{c}_{i+1/2} - \hat{c}_{i-1/2}), \tag{4}$$

where $\lambda = u\Delta t/\Delta x$ is the Courant number, in which Δt is the time step and Δx is the grid size. As mentioned in Eq. (1), the superscript n and subscript i of c denote the number of time steps and grid divisions, respectively. $\hat{c}$ denotes the approximated c value at the interfaces of the grid.

The key to the advection scheme is the determination of the interface value $\hat{c}$, which is related to the tracer flux. Based on the first-order upwind scheme and the second-order Lax-Wendroff scheme (Lax and Wendroff, 1960), Sweby (1984) constructed the temporal and spatial second-order TVD scheme, in which $\hat{c}$ is given by Eq. (5).

$$\hat{c}_{i+1/2} = \begin{cases} c_i^n + \frac{1}{2}\psi(r_{i+1/2}^+)(1-\lambda)(c_{i+1}^n - c_i^n), & \text{if} u_{i+1/2} \geq 0 \\ c_{i+1}^n - \frac{1}{2}\psi(r_{i+1/2}^-)(1+\lambda)(c_{i+1}^n - c_i^n), & \text{if} u_{i+1/2} < 0 \end{cases}, \tag{5}$$

where ψ is the function of the flux limiter and r denotes the ratio of the upwind gradient to the local gradient, as given below.

$$\begin{cases} r_{i+1/2}^+ = (c_i^n - c_{i-1}^n)/(c_{i+1}^n - c_i^n) \\ r_{i+1/2}^- = (c_{i+2}^n - c_{i+1}^n)/(c_{i+1}^n - c_i^n) \end{cases} \tag{6}$$

Sweby (1984) provided the region of the limiting function ψ for the TVD schemes for Eq. (5) and specifically the second-order region.

$$\begin{cases} 0 \leq \psi(r) \leq \min(2, 2r), & r > 0 \\ \psi(r) = 0, & r \leq 0 \end{cases} \tag{7}$$

Some typical flux limiters of Sweby's TVD schemes are shown in Table 1. The limiters include not only the classical ones, i.e., Superbee, Minmod, Van-Leer (or Harmonic), and MUSCL but also the newly proposed HSIMT. HSIMT, which is based on Kim and Kim's scheme (Kim and Kim, 2005), has spatial third-order accuracy (Wu and Zhu, 2010).

2.2. TVD with an alternating limiter (TVDal)

According to Table 1, the Superbee-TVD scheme is a compressive one, whereas the others are diffusive. Therefore, the use of an alternating limiter is proposed to balance the flux limiting, i.e., to neutralize compression and diffusion. Thus, the function of the limiter ψ can be constructed as

$$\psi(r) = \begin{cases} \psi^{com}, & n \text{ is odd} \\ \psi^{dif}, & n \text{ is even} \end{cases}, \tag{8}$$

where n is the time step, and ψ^{com} and ψ^{dif} represent compressive and diffusive limiters, respectively. In practice, exchanging the order of the compression and diffusion limiters has little effect on the results because a difference in a single step has a negligible effect on the total integration.

In this study, Superbee was used as the compressive limiter and was combined with different diffusive limiters, which is the key concept behind the TVDal scheme applied in this study. The flux limiter of the TVDal scheme is denoted by the prefix 'S-.' For example, S-MUSCL represents the TVDal scheme, wherein the Superbee and MUSCL flux limiters are alternatingly used.

The alternating flux limiter scheme comprises two different limiter schemes and uses different limiters in various time steps. Therefore, the efficiency of TVDal is the same as that of TVD.

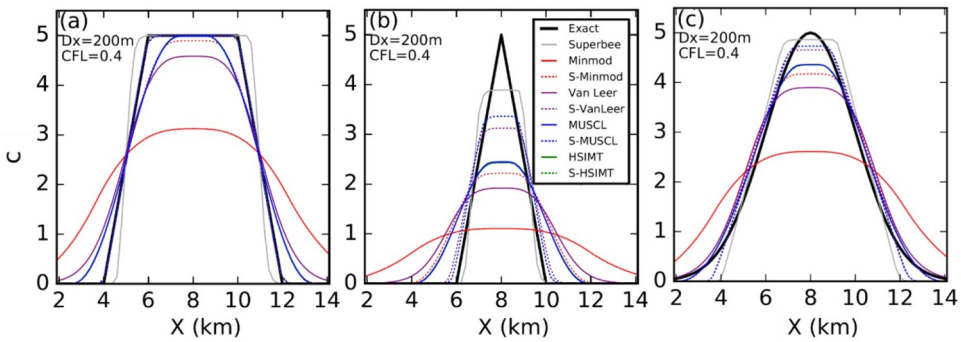

Fig. 1. Comparison of the numerical results at the 200th cycles of TVD schemes and TVDal schemes for the three distribution advections (Dx is the grid space). (a) trapezoidal shape, (b) triangular shape, (c) normal distribution. The black lines denote the three initial distributions of passive tracer c for the 1D benchmark test.

2.3. TVDal combined with the Strang splitting method

In the 2D benchmark experiment, the TVDal scheme was used to resolve 2D advection:

$$\frac{\partial c}{\partial t} + u\frac{\partial c}{\partial x} + v\frac{\partial c}{\partial y} = 0. \tag{9}$$

The direct application of TVD to the 2D simulation can still induce numerical dispersion (e.g., Strang, 1968; Leonard et al., 1996; Pietrzak, 1998), especially in long time simulations (Choi et al., 2018). To avoid numerical dispersion, the Strang splitting method (Strang, 1968) is used to construct the multi-dimensional advection scheme. The Strang splitting method splits the two directions of Eq. (9) into two steps and alternates the priority order of the calculation (Leonard et al., 1996; Cushman-Roisin and Beckers, 2011).

By adding the alternating flux limiters into the Strang splitting method, one can obtain the multi-dimensional TVDal scheme, and the calculation process of the Strang-splitting TVDal scheme is as follows:

$$\begin{cases} c_{i,j}^{*} = c_{i,j}^{n} - \lambda_x(\hat{c}_{x,i+1/2,j}^{com} - \hat{c}_{x,i-1/2,j}^{com})^n \\ c_{i,j}^{n+1} = c_{i,j}^{*} - \lambda_y(\hat{c}_{y,i,j+1/2}^{dif} - \hat{c}_{y,i,j-1/2}^{dif})^* \end{cases}, \quad n \text{ is odd}$$
$$\begin{cases} c_{i,j}^{*} = c_{i,j}^{n} - \lambda_y(\hat{c}_{y,i,j+1/2}^{com} - \hat{c}_{y,i,j-1/2}^{com})^n \\ c_{i,j}^{n+1} = c_{i,j}^{*} - \lambda_x(\hat{c}_{x,i+1/2,j}^{dif} - \hat{c}_{x,i-1/2,j}^{dif})^* \end{cases}, \quad n \text{ is even} \tag{10}$$

In the equation, the variables with subscript x (or y) denote the x-direction (or y-direction) component and c^* corresponds to the intermediate time steps between n and $n+1$. In this paper, $(\hat{c}_{y,i,j} - \hat{c}_{y,i,j})^n$ and $(\hat{c}_{y,i,j} - \hat{c}_{y,i,j})^*$ are identical to $(\hat{c}_{y,i,j}^{n} - \hat{c}_{y,i,j}^{n})$ and $(\hat{c}_{y,i,j}^{*} - \hat{c}_{y,i,j}^{*})$, respectively. The superscripts *com* and *dif* of $\hat{c}$ denote the use of compressive and diffusive limiters, respectively.

As shown in Eq. (10), advection in the x-direction is calculated first, and the intermediate value c^* is derived for one odd time step. The advection in the y-direction is then calculated. At the next time step, the calculation order is swapped, and the advection in the y-direction is calculated first. For the S-MUSCL scheme, the Superbee flux limiter is used in the x-direction, whereas the MUSCL limiter is used in the y-direction at the first step. At the next time step, the two flux limiters are used by alternating the directions.

2.4. Quantification of numerical error and variance conservation

The normalized root mean square error (*NRMSE*) was used to quantify the error of the advection scheme.

$$NRMSE = \sqrt{\frac{\sum_{i=1}^{N}(c_i^t - c_i^{a,t})^2}{\sum_{i=1}^{N}(c_i^{a,t})^2}}, \tag{11}$$

where N is the total number of grids and c_i^t and $c_i^{a,t}$ denote the simulated and analytic substance concentrations, respectively.

Several methods can be used to diagnose numerical diffusion (e.g., Klingbeil et al., 2014; Ilicak, 2016). In this study, the variance-variation diagnostic method (Wu and Zhu, 2010) was used. The variance conservation of each scheme was evaluated with the index *EV*:

$$EV = \frac{\sum_{i=1}^{N}(c_i^t)^2}{\sum_{i=1}^{N}(c_i^{a,t})^2} - 1. \tag{12}$$

The *EV* index can reflect the strength of the advection schemess compression or diffusion. If $EV > 0$, the scheme shows artificial steepening and is compressive. If $EV < 0$, the scheme is dissipative and diffusive. If $EV = 0$, the scheme conserves variance.

3. Benchmark experiments

Numerical experiments for idealized 1D and 2D advection were conducted to test the performances of the TVDal schemes by comparing them with the aforementioned conventional TVD schemes.

3.1. 1D experiment

3.1.1. Experiment configuration

The 1D linear moving-front tests used to test the TVDal schemes are described. Initially, a passive tracer distribution was specified in a 22-km channel. Three types of distributions, i.e., trapezoidal, triangular, and normal distributions, were used to represent normal, sharp, and smooth fronts, respectively (Fig. 1). In the channel, a spatially homogeneous, incompressible, and reversing flow field $u(x, t) = U\sin(2\pi t/T)$ existed, where U is the amplitude of a reversing flow such as a tidal current and T is the period of tidal flow. In the test, the variables U and T were set to 0.4 m/s and 12 h, respectively. Moreover, the tracer values at the two boundaries were set to zero. The channel was long enough such that a non-zero tracer could not reach the boundaries, and the effects of the boundary conditions could be ignored.

Assuming the initial tracer distribution is $c(x, t_0)$, the analytic distribution should be $c(x, t) = c\left(x - \int_{t_0}^{t} u(t')dt', t_0\right)$. Using a Lagrangian coordinate with the movement at a velocity of $U\sin(2\pi t/T)$, the tracer distribution at any time should be the same as that of the initial distribution.

Test cases with different grid spaces (100 m and 200 m) and three types of time steps Δt were utilized to check the advection schemes. The CFL criterion maxima, i.e., CFL=$U\Delta t/\Delta x$, were 0.8, 0.4, and 0.2 for the three types of time steps. All of the cases were run for 200 T.

3.1.2. Experiment results

Fig. 1 presents the results of the TVDal and TVD schemes for the 1D test cases. For the sake of simplicity, only the result of the case with Δx = 200m and CFL = 0.4 is shown because similar results were found

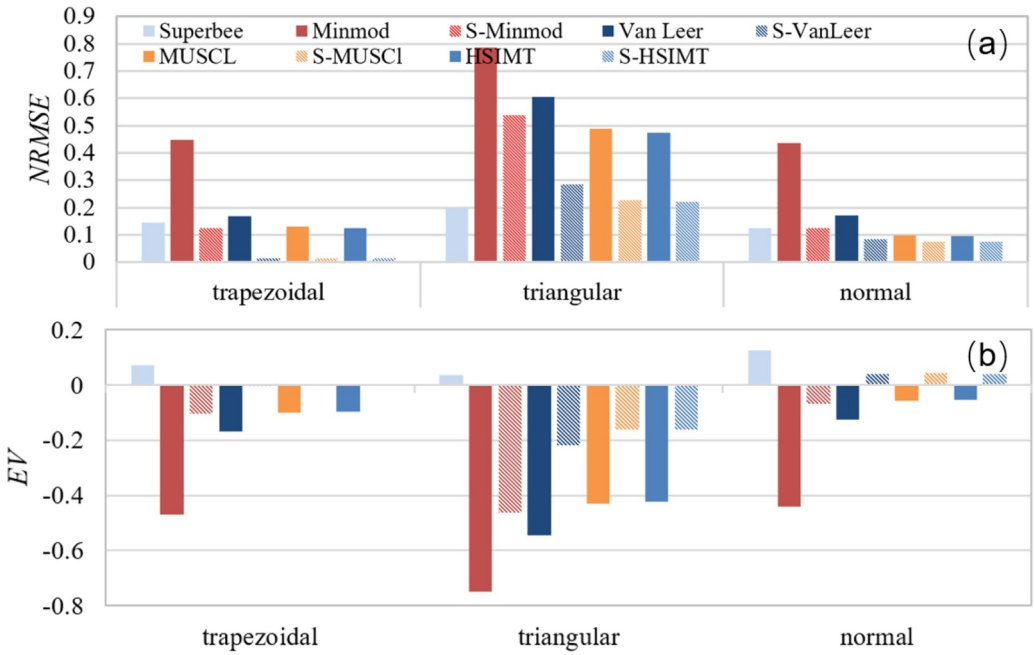

Fig. 2. The *NRMSE*s (a) and *EV*s (b) of TVD schemes and TVDal schemes for the simulation results in Fig. 1.

in other cases. More detailed results are included in Figs. S1-S4 in the Supplementary Information (SI). The results of the Superbee scheme demonstrated the numerical compression. The other conventional TVD schemes, i.e., Minmod, Van Leer, MUSCL, and HSIMT, exhibited numerical diffusion, particularly for the sharp-front cases, i.e., the triangular shape (Fig. 1b).

TVDal schemes showed improved results due to the counterbalance between the compression of the Superbee approach and the diffusion of the other methods. In particular, the *NRMSE*s for the coarse-grid cases were reduced by approximately 56% (Fig. 2a). The S-Minmod scheme significantly reduced the strong numerical diffusion of the Minmod scheme and produced a similar result to those of the MUSCL and HSIMT schemes. Although the results of the traditional Van Leer scheme were poor relative to MUSCL and HSIMT, the performance of the modified scheme (i.e., S-VanLeer) was better. The results for both the S-MUSCL and S-HSIMT schemes approached the analytic solution, especially for the trapezoidal case (Fig. 1a). Although these two TVDal schemes had slight compressions in the smooth case, the compressions were significantly less than that of the Superbee method, and the maxima were basically maintained (Fig. 1c).

The *EV* results could explain the improvements in the simulations when using the TVDal schemes in comparison with the TVD schemes. For brevity, the S-MUSCL scheme was selected as an example for analysis. As shown in Fig. 2b, all of the *EV*s for the Superbee and MUSCL schemes were positive and negative, respectively, indicating the compression of the Superbee scheme and the diffusion of the MUSCL scheme. In the trapezoidal cases, the S-MUSCL *EV*s were close to zero (<0.01), indicating that the alternating flux limiter perfectly balanced the Superbee compression and MUSCL diffusion. Therefore, the simulation resulted in a substantial improvement, with a reduction in *NRMSE*s. For the sharp triangular cases, there was excessive diffusion under the diffusive TVD schemes, which indicated that Superbee compression was insufficient to balance MUSCL diffusion using the alternating flux limiter S-MUSCL scheme. For the normal distribution cases, the compression of the Superbee scheme was over-balanced by the diffusion of the MUSCL scheme, which caused S-MUSCL to be slightly compressive. Therefore, the S-MUSCL results for the triangular and normal distribution cases exhibited smaller improvements than for trapezoidal cases.

Overall, for all 1D test cases, the *NRMSE* of TVDal schemes was decreased by an average of ~60% compared to the original TVD schemes. These results suggested that advection schemes with alternating flux limiters could efficiently improve the numerical results of the original schemes by balancing numerical compression and diffusion.

3.2. 2D experiment

3.2.1. Experimental configuration

In 2D test cases, oblique advection at an angle of 45° for a reversed U-shaped distribution (Fig. 3a) (a slotted circular truncated cone similar to the idealized experiment by Pietrzak, 1998) and with a horizontal resolution of 100 m was conducted in a 30 km × 30 km domain. A horizontal uniform and reversing flow field with $\vec{v}(x, y, t) = \vec{V}\sin(2\pi t/T)$ was provided, where the direction of the vector $\vec{V}$ was northeastwards, and T was the period of reverse flow. The variables $|\vec{V}|$ and T were set to 0.4 m/s and 12 h, respectively, in all the 2D test cases. As in the preceding 1D experiments, the analytic distribution by advection should be the same in terms of the initial distribution at any time using the Lagrangian coordinate. Assuming the initial tracer distribution is $c(x, y, t_0)$, the analytic distribution should be $c(x, y, t) = c\left(x - \int_{t_0}^{t} u(t')dt', y - \int_{t_0}^{t} v(t')dt', t_0\right)$. Simulation results at 100-s time steps over 100 T were obtained.

3.2.2. Experimental results

For brevity, only the Superbee, MUSCL, and S-MUSCL results are shown in Fig. 3, and others are provided in Fig. S5 in the SI. Fig. 3b and c clearly show that the results of 2D TVD schemes without the splitting method were strongly dispersive and cannot guarantee the non-oscillatory property of the TVD scheme, as reported by Goodman and LeVeque (1985). Therefore, it is of critical importance to employ the splitting method for extending the 1D advection scheme to 2D. The results of the Superbee scheme showed the serious distortion induced by strong artificial steepening (Fig. 3d). The MUSCL scheme retained the peripheric circle shape of the distribution, whereas its numerical diffusion resulted in mixing, particularly around the bottom of the U-shape (Fig. 3e). The result of the S-MUSCL scheme accurately retained the U-shape and had smaller errors than the MUSCL scheme, although there was a slight change in shape around the inner high value (Fig. 3f).

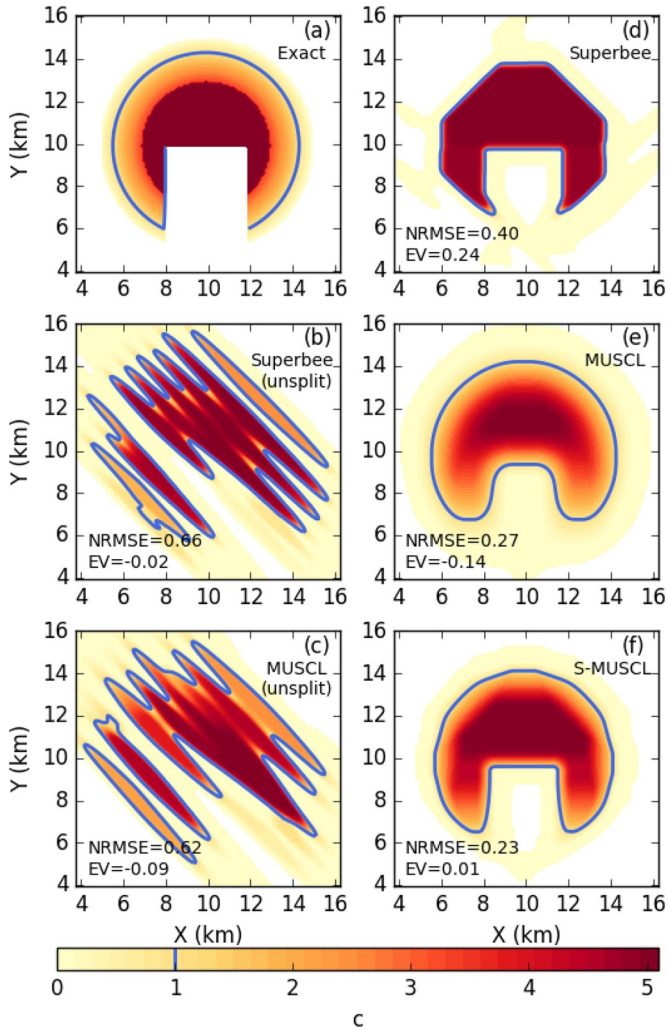

Fig. 3. 2D advection simulation results at the 100th cycle (the blue line shows the contour line of 1). (a) is analytic solution. (b) and (c) are the results of Superbee and MUSCL TVD schemes without the splitting method, respectively. (e)and (f) (~~b~~) and (~~c~~) are the results of Superbee and MUSCL TVD schemes with the Strang-splitting method, respectively. ~~(d) is the results of the S-MUSCL TVDal scheme~~.

The *NRMSE* of the S-MUSCL scheme was reduced by ~15% relative that of the HSIMT scheme. In addition, the *EV* absolute value for the S-MUSCL was only 0.01, which was greatly reduced when compared to MUSCL (0.14) and Superbee (0.24). Overall, the TVDal schemes performed better than the traditional TVD schemes; the *NRMSE* of TVDal schemes decreased by an average of ~24% compared to that of the original TVD schemes in the 2D case. These results demonstrated that TVDal could efficiently reduce numerical error in multi-dimensional cases.

4. Simulation of tidally induced internal lee waves

In addition to the benchmark tests, the TVDal schemes were also applied to model tidally induced internal waves. This case featured nonlinearity, strong stratification, and non-uniform incompressible flow fields. In the horizontal 2D benchmark experiment, the Strang splitting method was stable because of the linearity and the spatially homogeneous flow field. However, realistic ocean modelling often must address inhomogeneous flow fields. In such cases, the Strang splitting method could result in instability due to the inconstancy-preserving advection problem (e.g., Leonard et al., 1996). To overcome this problem, TVDal in conjunction with the splitting method of Pietrzak (1998) for ocean models with a σ-coordinate system was applied in the Marine Environment Research and Forecast model (MERF) developed by Liu et al. (2016), which was used for the test case of a tidally induced internal lee wave. In the 3D model, the limiter alternating sequence was *x-σ-y, y-σ-x, x-y-σ, σ-y-x, y-x-σ*, and *σ-x-y*, with the sequence cycles in that order. According to that order, the *x, y*, and *σ* directional calculations could occur at the first, second, and third sequences, respectively, with the same frequencies. TVDal was only used for the advection of temperature. Other algorithms and details of the MERF solution procedure were introduced in Liu et al. (2016, see Sections 2 and 3).

The model configuration and initial conditions were set according to Xing and Davies (2006) and Berntsen et al. (2009). The initial temperature linearly decreased from sea surface to sea floor, and the salinity was spatially uniform and kept constant. The model domain was discretized with a uniform grid spacing of 10 m in the horizontal direction and 40 uniform σ-layers in the vertical direction. A time step of 0.2 s was used. The western open boundary of the domain was driven by an M_2 tide by specifying a velocity of u = 0.3sin(0.000140526*t*) m/s. The experiments were performed with constant values of 10^{-7} m^2/s for both the horizontal and vertical diffusivities, as in Xing and Davies (2006). Therefore, advection played a dominant role in the transport of cold water in vortexes and temperature field variations.

Five TVD schemes and four TVDal schemes were used for modeling temperature advection in the internal lee wave experiment. All of the experiments showed that during the flood stage, the flow separation near the top of the sill resulted in convective vortexes above the oscillation of the isotherms at the downstream side of the sill (for brevity, only the Superbee, MUSCL, and S-MUSCL results are shown in Fig. 4, and other results are provided in Figs. S6-S7 in the SI). The cold water (temperature < 11.5 °C) vortexes generated and propagated above −50 m water depth at the downstream side of the sill. The results were consistent with those of previous modeling studies (e.g., Xing and Davies, 2006).

The temperature distributions simulated using the different schemes at 1/4 and 1/2 of the tidal cycle are shown in Fig. 4. According to the Superbee TVD simulation results (Fig. 4a and b), the cold water mass was transported downstream by approximately 1800 m because of its anti-diffusion characteristics. However, the cold vertexes simulated using MUSCL TVD schemes did not reach as far as a result of numerical diffusion (see Fig. 4d). In Fig. 4, the right dashed boxes show the large differences in the modeling results within the region where $X \in [1200, 1800]$ m. The results of the TVDal schemes revealed that the cold water in the vortexes extended to $X \in [1200, 1800]$ *m* (see Fig. 4e f), indicating that the numerical diffusion was reduced compared to the original diffusive TVD schemes. The minimum water temperature (MWT) values in the cold vortices in the region of different schemes are shown in Fig. 5a. The MWT values from the compressive Superbee scheme were the lowest, whereas those from the diffusive scheme were relatively high. TVDal, which could balance the compression and diffusion, had intermediate values for MWT.

In addition, the increased potential energy (IPE) induced by the vertical variation in water density for the region of $X > 0$ m was calculated using

$$IPE(t) = g\int\int\int[\rho(t)z(t)]\mathrm{d}V - g\int\int\int[\rho(0)z(0)]\mathrm{d}V - g\int\int\int[\rho_0(z(t)-z(0))]\mathrm{d}V, \quad (13)$$

where ρ(*t*) and *z*(*t*) are the water potential density and the potential height, respectively, at moment *t*, ρ(0) and *z*(0) denote the initial water potential density and potential height, respectively, and ρ_0 is the reference density. The third term on the right-hand side denotes that the increase in potential energy induced by the increase of water level is removed. Therefore, IPE is the increased potential energy due solely to the vertical variation in water density. Fig. 5b shows the differences among the IPEs for the different schemes increased with time, which

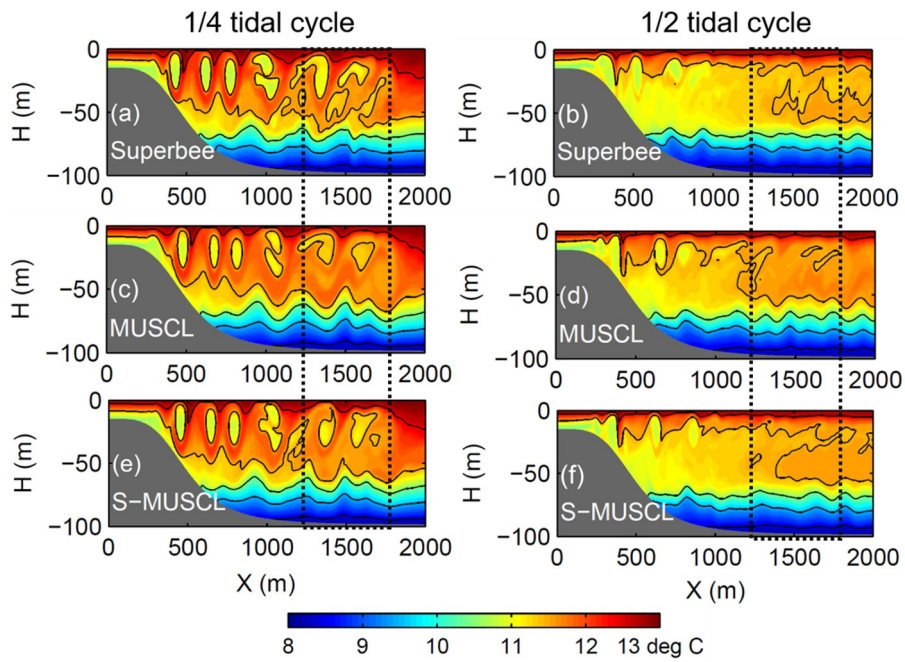

Fig. 4. Snapshots of the temperature distributions at 1/4 (a, c, and e) and 1/2 (b, d, and f) of the tidal cycle obtained from the different advection schemes. From the bottom up, the black lines are the 8.5, 9.5, 10.5, 11.5 and 12.5 °C contours. The black dashed boxes show the region from x = 1200–1800 m.

means that the impact of using different advection schemes on the simulation result could increase gradually. At a 1/4 tidal cycle, the difference between Superbee and Minmod reached $\sim 0.3 \times 10^7$ J, which was ~10% of the IPE ($\sim 3.2 \times 10^7$ J on average). The diffusive schemes had higher IPEs due to increased diffusion, which resulted in more vertical mixing. The compressive Superbee schemes had relatively lower IPEs. Basically, the IPEs of the TVDal schemes were between those of the diffusive and Superbee schemes. This was consistent with the performance of TVDal in previous idealized test cases (e.g., the *EV* variations shown in Fig. 2).

Because there were no analytic solutions or lab or field data, it cannot be concluded which of the advection schemes produced the best results for the lee wave case, but the results suggest that TVDal could balance the diffusion and compression from different TVD limiters in a similar way to that in the 1D test case. Therefore, TVDal is a potential method for resolving the issue of numerical diffusion and compression

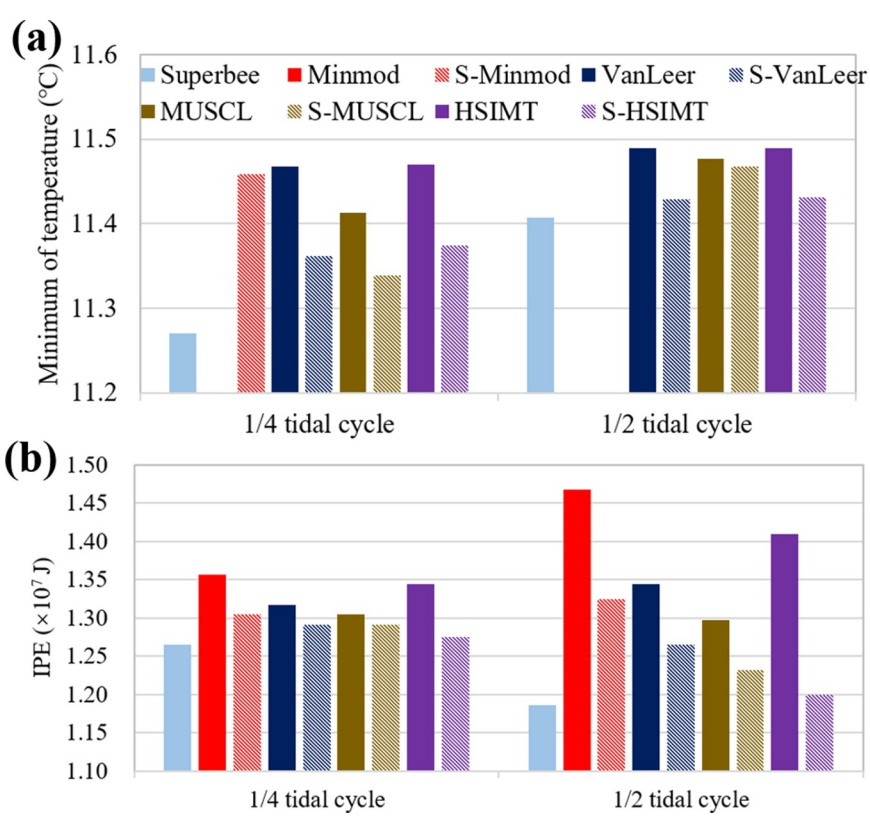

Fig. 5. (a) The minimum temperatures of the vortices in the region from x = 1200–1800 m for the test case of tidally induced internal waves. The missing bars denote that were no cold vortices (< 11.5 °C) when using the related advection scheme. (b) The increased potential energy (IPE) from the different schemes. Note that IPEs in the 1/2 tidal cycle are reduced by 1.94×10^7 J for comparison with that in 1/4 tidal cycle.

Table 2
The optimal *SR*s for TVDal schemes and the reduced error by TVDal.

Test cases	Triangular				Trapezoidal				Normal			
TVDal Schemes	S-Minmod	S-VanLeer	S-MUSCL	S-HISMT	S-Minmod	S-VanLeer	S-MUSCL	S-HISMT	S-Minmod	S-VanLeer	S-MUSCL	S-HISMT
The optimal *SR*	14/1	6/1	3/1	3/1	3/1	1/1	1/1	1/1	3/1	1/1	1/2	1/2
Reduced *NRMSE* by the optimal *SR*	75.8%	69.2%	63.1%	60.3%	96.7%	91.1%	89.2%	90.0%	80.0%	50.2%	22.2%	20.1%
Reduced *NRMSE* by 1/1 *SR*	35.3%	54.2%	54.6%	51.2%	72.1%	91.1%	89.2%	90.0%	71.1%	50.2%	21.9%	20.0%
***EV* of the optimal SR**	−0.027	−0.031	−0.048	−0.047	0.000	−0.001	0.001	0.000	0.042	0.040	0.028	0.029
***EV* of 1/1 SR**	−0.465	−0.218	−0.162	−0.161	−1.042	−0.001	0.001	0.000	−0.067	0.040	0.041	0.040

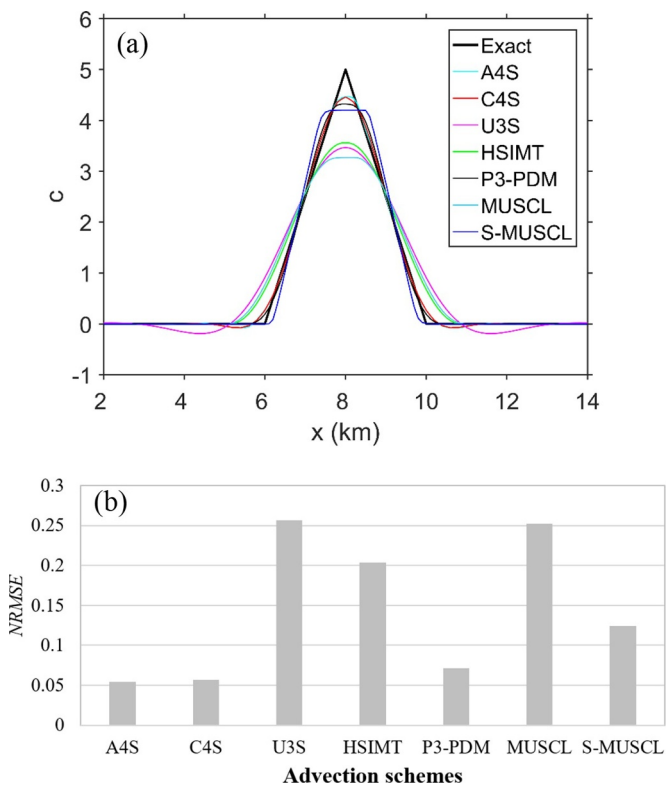

Fig. 6. (a) Comparison of the S-MUSCL TVDal scheme with higher-order schemes, including the 4th-order Akima scheme (A4S), 4th-order centered scheme (C4S), 3rd-order upwind scheme (U3S), 3rd-order HSIMT scheme, 4th-order upwind scheme with TVD limiter (P3-PDM), and 2nd-order MUSCL TVD scheme. (b) The root mean square errors (*NRMSE*s) of the different schemes.

induced by conventional TVD schemes.

5. Discussion

5.1. Combining ratios of the compressive and diffusive limiters

In the experiments above, the combining ratio was 1/1 for the compressive and diffusive limiters. A TVDal with a combining ratio of 1/1 probably cannot produce a maximum benefit because it may not completely counterbalance compression and diffusion due to their different strengths. Therefore, in this section, different combining ratios are tested to find the optimal ratio and evaluate the performance of TVDal with a ratio of 1/1 by comparing it with the optimal solution.

Defining *SR* as the ratio of the time step number of the Superbee-limiter to that of a diffusive limiter, the three idealized 1D test cases with different shapes introduced in Section 3.1 were simulated by different TVDal schemes with different *SR*s varying from 20/1 to 1/20. The optimal *SR* with a minimum *NRMSE* and its reduction of *NRMSE* for different TVDal schemes are listed in Table 2. In most cases, the optimal *SR*s are approximately 1/1 (basically from 3/1 to 1/2), except in the sharp triangle test case, for which relatively strong diffusive Minmod and VanLeer schemes require a higher *SR* than in other cases. However, 1/1 *SR* can also significantly reduce the *NRMSE*s of original schemes in those two cases (35.3% and 54.2%, respectively). In general, the optimal *SR*s can reduce the *NRMSE*s of original schemes by an average of ~67%, while TVDal with 1/1 *SR* can achieve an average ~58% *NRMSE* reduction, which is very close to the optimal *SR*. Therefore, the performance of TVDal with 1/1 *SR* is generally acceptable, and to avoid having to select *SR*, the alternating limiter with 1/1 *SR* is recommended in practice. In fact, *NRMSE* did not significantly decrease as *SR* varied from 1/1 to the optimal *SR*, even though *EV* was closest to zero (Table 2). The reason was that the finite accuracy limited the reduction in numerical error, and the numerical error could not converge with the decrease in *EV* in this case.

5.2. Comparison with high-order schemes

With increasing computational power, high-order advection schemes with less diffusion and compression have been gradually adopted in community ocean models such as the third-order upwind-biased scheme used in the Modular Ocean Model (MOM) and Regional Ocean Modeling System (ROMS) (e.g., Griffies, 2009; Naughten et al., 2017) and the fourth-order Akima and centered advection scheme implemented in ROMS (e.g., Naughten et al., 2017). To investigate the differences between TVDal and higher-order schemes, the second-order S-MUSCL TVDal scheme was compared with the higher-order schemes with and without limiters, including a fourth-order Akima scheme (A4S, used in ROMS), a fourth-order centered scheme (C4S, used in ROMS), a third-order upwind scheme (U3S, used in ROMS and MOM), the third-order HSIMT scheme based on Kim and Kim (2005) and proposed by Wu and Zhu (2010), and high-order upwind schemes with TVD limiters from Pietrzak (1998), i.e., the fourth-order P3-PDM.

According to the results of the 1D benchmark tests, the *NRMSE*s of the TVDal schemes for the 1D triangle case were obviously greater than in the other two cases. Therefore, the triangle case was adopted for comparison. As shown in Fig. 6, S-MUSCL TVDal outperformed the third-order HSIMT and U3S, with an *NRMSE* reduction of 0.11, but was inferior to the fourth-order P3-PDM schemes, with *NRMSE* increases of 0.05. Generally, the fourth-order schemes (i.e., A4S, C4S, and P3-PDM) produced better results than S-MUSCL and other relatively lower-order schemes in the range of 6–10 km. However, A4S and C4S showed ~1 km-long negative values due to their dispersion, whereas P3-PDM was positive definite but had slightly higher (~0.02) *NRMSE* than those of A4S and C4S (Fig. 6b). It should be noted that the S-MUSCL TVDal is of second-order accuracy and costs only ~50% of the CPU consumption of the fourth-order schemes. In addition, there are some potential difficulties when applying higher-order schemes in unstructured meshes due to their use of greater numbers of nodes. By adding another flux limiter, TVDal can be easily used or integrated into ocean models using TVD schemes without additional computations.

5.3. Potential of applying TVDal in high-order TVD schemes

According to Tseng (2008), the higher-order schemes could cause

oscillations and overshooting under highly convective conditions, resulting in unphysical effects, while high-order schemes with TVD limiters (e.g., the fourth-order P3-PDM in this study) can eliminate unphysical effects. The above results (Fig. 6) also suggest that TVDal would be limited by the finite accuracy of the TVD limiters used. Hence, the Superbee scheme was combined with fourth-order P3-PDM, which has relatively less diffusion, to investigate whether TVDal works for high-order TVD schemes. The *NRMSEs* and *EVs* for the different *SRs* of Superbee and P3-PDM showed that the minimum *NRMSE* was at $SR = 1/200$, where *EV* was almost zero. The *NRMSE* of TVDal with $SR = 1/200$ was ~ 0.063, which was $\sim 11\%$ less than that of P3-PDM (~ 0.071). The results suggest that TVDal with an *SR* of 10^{-2} order can also improve higher-order TVD schemes to some extent, although the improvements will be less than those for lower-order schemes. This might be because the compressive limiter used in TVDal was still the second-order Superbee limiter, which has finite accuracy. Replacing the Superbee limiter by a higher-order compressive limiter should improve higher-order TVD schemes more significantly.

5.4. Local extrema 'clipping'

The modeling results of the 1D triangular case indicate that the TVD schemes suffer from a well-known inherent drawback in that even the high-order TVD schemes degrade to first order at local extrema and produce unphysical 'clipping' at local extrema (e.g., Yang and Przekwas, 1992; Leonard et al., 1996). Because r in Eq. (7) near the local extrema is negative or zero, which means that the limiter $\psi(r) = 0$ (see Eq. (7)), the TVD scheme will become a first-order upwind scheme near local extrema.

This TVD 'clipping' defect also influenced the fourth-order P3-PDM scheme, which resulted in a lower maximum (Fig. 6a) and higher *NRMSE* (Fig. 6b) than those of the fourth-order A4S and C4S schemes. TVDal also suffers this defect because it does not make an intrinsic change to the TVD limiters, which still equal zero at local maxima. To address this problem of TVD-type schemes, ENO/WENO schemes have been proposed, which are not required to degrade at the local extrema (e.g., Harten et al., 1987; Shi et al., 2002; Zhang et al., 2015). However, ENO/WENO schemes need a larger finite-difference stencil than the traditional TVD schemes, which have more computational costs and become extremely challenging in applications near ocean boundaries and on unstructured meshes (e.g., Arora and Roe, 1997; Zhang et al., 2015). This is the possible reason for the limited application of ENO/WENO in ocean modelling.

6. Conclusions

Although TVD schemes are widely used in ocean modelling, numerical errors still occur due to compression or diffusion by different flux limiters. To eliminate these numerical errors, TVDal is proposed.

The TVDal schemes were tested in 1D and 2D advection cases. In the 1D test, TVDal produced a smaller error than the original schemes for both the normal and sharp front cases. In general, TVDal can reduce *NRMSE* by $\sim 60\%$. In 2D cases, the TVD schemes were coupled with the Strang-splitting method. The Strang-splitting TVDal can better maintain advection and the TVD property, which is not strictly retained by Strang-splitting Superbee. The TVDal scheme also shows an ability to balance compression and diffusion induced by TVD advection schemes for applications to simulations of tidally induced internal lee waves, a case that features highly nonlinear, stratified, and nonhomogeneous flow fields, showing the potential application of TVDal to ocean modelling under realistic conditions. The test results indicate the 1/1 *SR* is the practical optimal strategy for combining compressive and diffusive limiters if they are of the same order. In the meantime, if the limiters have different orders, the step ratio of higher-order to lower-order limiters should be adjusted accordingly.

Acknowledgments

MERF has been upgraded from MERF-NH 1.0 (MERF Non-hydrostatic Version 1.0; Liu et al., 2016) to MERF-NH 2.0 primarily because of the adoption of the SS-TVDal method instead of the Superbee TVD scheme. The program used in this study is based on MERF-NH 2.0. For access to MERF-NH 2.0 and the associated data, please contact zliu@ouc.edu.cn.

The authors thank Profs. Huiwang GAO and Lian XIE of the Ocean University of China, Prof. Xuefeng ZHANG of the National Marine Data and Information Service, and Profs. Dongyan LIU and Hui WU of the East China Normal University for their valuable suggestions. The authors also appreciate the insightful suggestions and comments of Editor Sergey Danilov and the two anonymous reviewers.

Supplementary materials

Supplementary material associated with this article can be found, in the online version, at doi:10.1016/j.ocemod.2019.01.002.

References

Arora, M., Roe, P.L., 1997. A well-behaved TVD limiter for high-resolution calculations of unsteady flow. J. Comput. Phys. 132 (1), 3–11.
Bernard, B., et al., 2006. . Erratum: impact of partial steps and momentum advection schemes in a global ocean circulation model at eddy-permitting resolution (Ocean Dynamics (2009) 59 (537)). Ocean Dyn. 56 (5–6), 543–567.
Berntsen, J., Xing, J., Davies, A.M., 2009. Numerical studies of flow over a sill: sensitivity of the non-hydrostatic effects to the grid size. Ocean Dyn. 59 (6), 1043–1059.
Boris, J.P., Book, D.L., 1973. Flux-corrected transport. I. SHASTA, a fluid transport algorithm that works. J Comput. Phys. 11 (1), 38–69.
Choi, Y.K., Shi, F., Malej, M., Smith, J.M., 2018. Performance of various shock-capturing-type reconstruction schemes in the Boussinesq wave model, FUNWAVE-TVD. Ocean Modell. 131, 86–100.
Cushman-Roisin, B., Beckers, J.M., 2011. Introduction to Geophysical Fluid dynamics: Physical and Numerical Aspects. Academic Press, pp. 192.
Fringer, O.B., Armeld, S.W., Street, R.L., 2005. Reducing numerical diusion in interfacial gravity wave simulations. Int. J. Numer. Methods Fluids 49, 301329.
Gerdes, R., Köberle, C., Willebrand, J., 1991. The influence of numerical advection schemes on the results of ocean general circulation models. Clim. Dyn. 5 (4), 211–226.
Goodman, J.B., Leveque, R.J., 1985. On the accuracy of stable schemes for 2D scalar conservation laws. Mathe. Comput. 45 (171), 15–21 1985, 595.
Griffies, S.M., 2009. ELEMENTS OF MOM4p1.
Harten, A., 1983. High resolution schemes for hyperbolic conservation laws. J Comput. Phys. 49 (3), 357–393.
Harten, A., Engquist, B., Osher, S., et al., 1987. Uniformly high order accurate essentially non-oscillatory schemes, III. J. Comput. Phys. 71 (2), 231–303.
Hecht, M.W., Bryan, F.O., Holland, W.R., 1998. A consideration of tracer advection schemes in a primitive equation ocean model. J. Geophys. Rese. 103 (C2), 3301–3321.
Ilicak, M., 2016. Quantifying spatial distribution of spurious mixing in ocean models. Ocean Modell. 108 (2016), 30–38.
Jeng, Y.N., Payne, U.J., 1995. An adaptive TVD limiter. J. Comput. Phys. 118 (2), 229–241.
Kim, K.H., Kim, C., 2005. Accurate, efficient and monotonic numerical methods for multi-dimensional compressible flows: Part II: Multi-dimensional limiting process. J. Comput. Phys. 208 (2), 570–615.
Klingbeil, K., Mohammadi-Aragh, M., Gräwe, U., Burchard, H., 2014. Quantification of spurious dissipation and mixing discrete variance decay in a finite-volume framework. Ocean Modell. 81 (2014), 49–64.
Lax, P., Wendroff, B., 1960. Systems of conservation laws. Commun. Pure Appl. Math. 13 (2), 217–237.
Leonard, B.P., Lock, A.P., Macvean, M.K., 1996. Conservative explicit unrestricted-time-step multidimensional constancy-preserving advection schemes. Mon. Weather Rev. 124 (11), 2588.
Lévy, M., Estublier, A., Madec, G., 2001. Choice of an advection scheme for biogeochemical models. Geophys. Res. Lett. 28 (19), 3725–3728.
Liu, G., Xue, H., 2009. The sensitivity of a 3D biogeochemical-like tracer model to advection schemes. Ocean Modell. 29 (4), 234–247.
Liu, Z., Lin, L., Xie, L., Gao, H., 2016. Partially implicit finite difference scheme for calculating dynamic pressure in a terrain-following coordinate non-hydrostatic ocean model. Ocean Modell. 106, 44–57.
Mercier, C.Y.M., Delhez, E.J.M., 2010a. Really TVD advection schemes for the depth-integrated transport equation. Ocean Model. 33 (1), 10–19.
Mercier, C.Y.M., Delhez, E.J.M., 2010b. A modified TVD scheme for the advection of two or more variables with consideration for their sum. Ocean Dyn. 60 (5), 1157–1166.
Mohammadi-Aragh, M., Klingbeil, K., Brüggemann, N., Eden, C., Burchard, H., 2015. The impact of advection schemes on restratification due to lateral shear and baroclinic

instabilities. Ocean Modell. 94, 112–127.
Naughten, K.A., Galton-Fenzi, B.K., Meissner, K.J., et al., 2017. Spurious sea ice formation caused by oscillatory ocean tracer advection schemes. Ocean Model. 116, 108–117.
Pietrzak, J., 1998. The use of TVD limiters for forward-in-time upstream-biased advection schemes in ocean modeling. Mon. Weather Rev. 126 (3), 812–830.
Roe, P.L., 1985. Some contributions to the modelling of discontinuous flows. Lectures in Applied Mathematics. pp. 163–193.
Shi, F., Kirby, J.T., Harris, J.C., Geiman, J.D., Grilli, S.T., 2012. A high-order adaptive time-stepping TVD solver for Boussinesq modeling of breaking waves and coastal inundation. Ocean Model. s43–s44 (2), 36–51.
Shi, J., Hu, C., Shu, C.W., 2002. A technique of treating negative weights in WENO schemes. J. Comput. Phys. 175 (1), 108–127.
Shi, J., Shi, F., Kirby, J.T., Ma, G., Wu, G., Tong, C., Zheng, J., 2015. Pressure Decimation and Interpolation (PDI) method for a baroclinic non-hydrostatic model. Ocean Modell. 96, 265–279.
Sommer, J.L., Penduff, T., Theetten, S., 2009. How momentum advection schemes influence current-topography interactions at eddy permitting resolution. Ocean Modell. 29 (1), 1–14.
Strang, G., 1968. On the construction and comparison of difference schemes. SIAM J. Numer. Anal. 5 (3), 506–517.
Sweby, P.K., 1984. High resolution schemes using flux limiters for hyperbolic conservation laws. SIAM J. Numer. Anal. 21 (5), 995–1011.
Tseng, Y.H., 2008. High-order essentially local extremum diminishing schemes for environmental flows. Int. J. Numer. Methods Fluids 58 (2), 213–235.
Van Leer, B., 1974. Towards the ultimate conservative difference scheme. II. Monotonicity and conservation combined in a second-order scheme. J. Comput. Phys. 14 (4), 361–370.
Van Leer, B., 1977. Towards the ultimate conservative difference scheme. IV. A new approach to numerical convection. J. Comput. Phys. 23 (3), 276–299.
Winther, N.G., Morel, Y.G., Evensen, G., 2007. Efficiency of high order numerical schemes for momentum advection. J. Mar. Syst. 67 (1–2), 31–46.
Wu, H., 2015. Cross-shelf penetrating fronts: a response of buoyant coastal water to ambient pycnocline undulation. J. Geophys. Res. Oceans 120 (7), 5101–5119.
Wu, H., Zhu, J., 2010. Advection scheme with 3rd high-order spatial interpolation at the middle temporal level and its application to saltwater intrusion in the Changjiang Estuary. Ocean Modell. 33 (1), 33–51.
Wu, H., Zhu, J., Shen, J., Wang, H., 2011. Tidal modulation on the Changjiang River plume in summer. J Geophys. Res. Atmos. 116 (C8), 192–197.
Xing, J., Davies, A.M., 2006. Processes influencing tidal mixing in the region of sills. Geophys. Res. Lett. 33 (4).
Yang, H.Q., Przekwas, A.J., 1992. A comparative study of advanced shock-capturing shcemes applied to Burgers' equation. J. Comput.Phys. 102 (1), 139–159.
Zalesak, S.T., 1987. A preliminary comparison of modern shock-capturing schemes: linear advection. Advances Comput. Methods PDEs. P15–P22 Publ. IMACS.
Zalesak, S.T., 1979. Fully multidimensional flux-corrected transport algorithms for fluids. J. Comput. Phys. 31 (3), 335–362.
Zhang, D., Jiang, C., Liang, D., Cheng, L., 2015. A review on TVD schemes and a refined flux-limiter for steady-state calculations. J. Comput. Phys. 302, 114–154.

Supporting Information for

TVDal: Total Variation Diminishing Scheme with Alternating Limiters to Balance Numerical Compression and Diffusion

Lei Lin[1, 2], Zhe Liu[2, *, ++]

[1]State Key Laboratory of Estuarine and Coastal Research, East China Normal University, Shanghai 200062, China
[2]Key Laboratory of Marine Environment and Ecology (Ocean University of China), Ministry of Education, Qingdao 266100, China

*Corresponding author
Zhe LIU
Key Laboratory of Marine Environment and Ecology (Ocean University of China), Ministry of Education, 238 Songling Road, Qingdao 266100, China
Email: zliu@ouc.edu.cn; Tel.: 86-532-66786568; Fax: 86-532-66782810;
++Now works in the Department of Earth Sciences, National Natural Science Foundation of China

Contents of this file

Introduction

This supplemental material includes seven figures for the detailed results of testcases.

Figs. S1-S3 show the results of three 1D test cases of TVD and TVDal schemes for different CFL values and grid spaces. Their NRMSEs and EVs are shown in Fig. S4.
Fig. S5 shows the results of the 2D test case achieved by all the tested TVD and TVDal schemes in this study, with the results of unsplit TVD schemes as well.
Figs. S6-S7 show the lee waves simulation results achieved by all the tested schemes in this study.

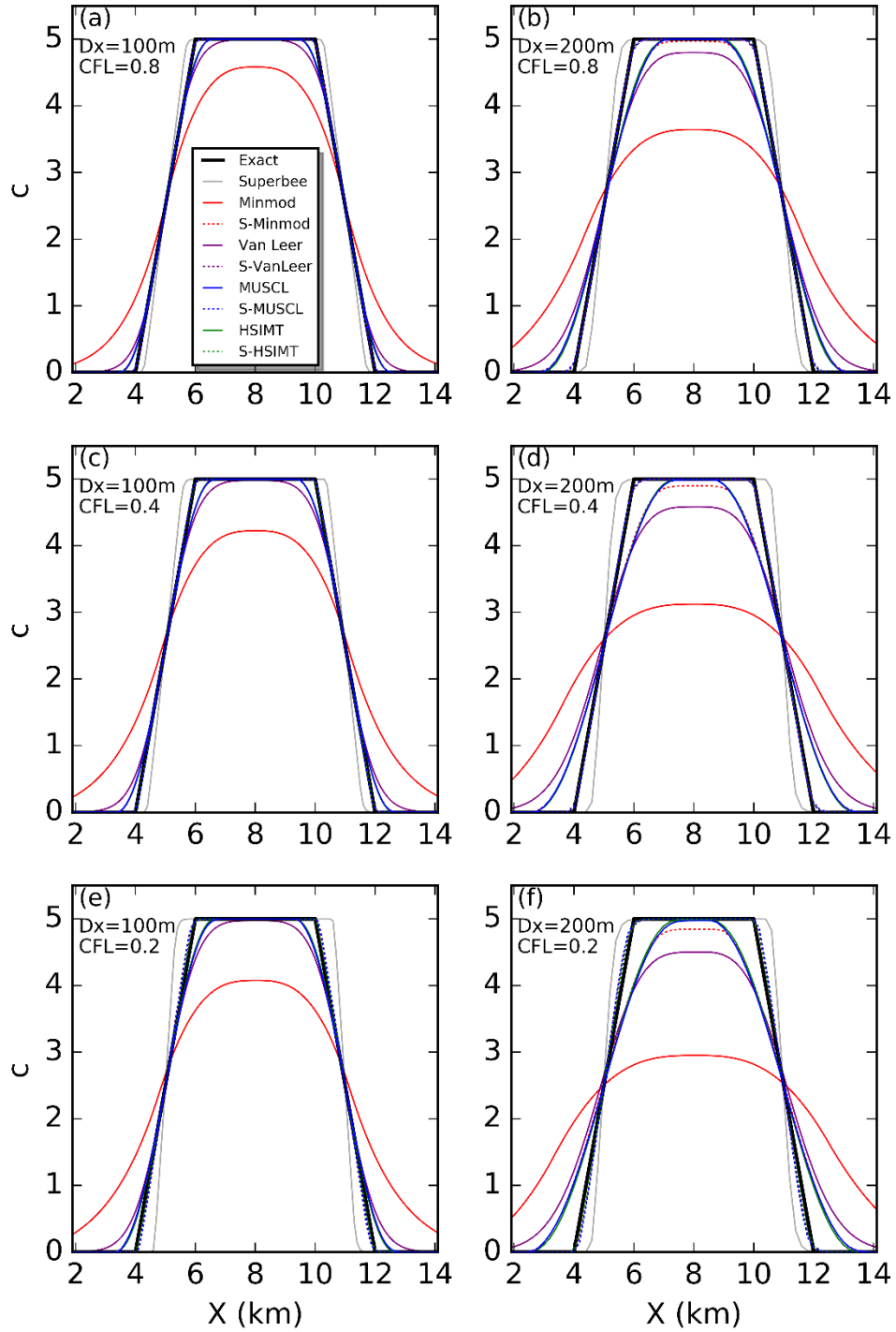

Fig. S1. Comparisons of the numerical results at the 200th cycles from the TVDal schemes and other schemes for the trapezoidal distribution advection (Dx is the grid space).

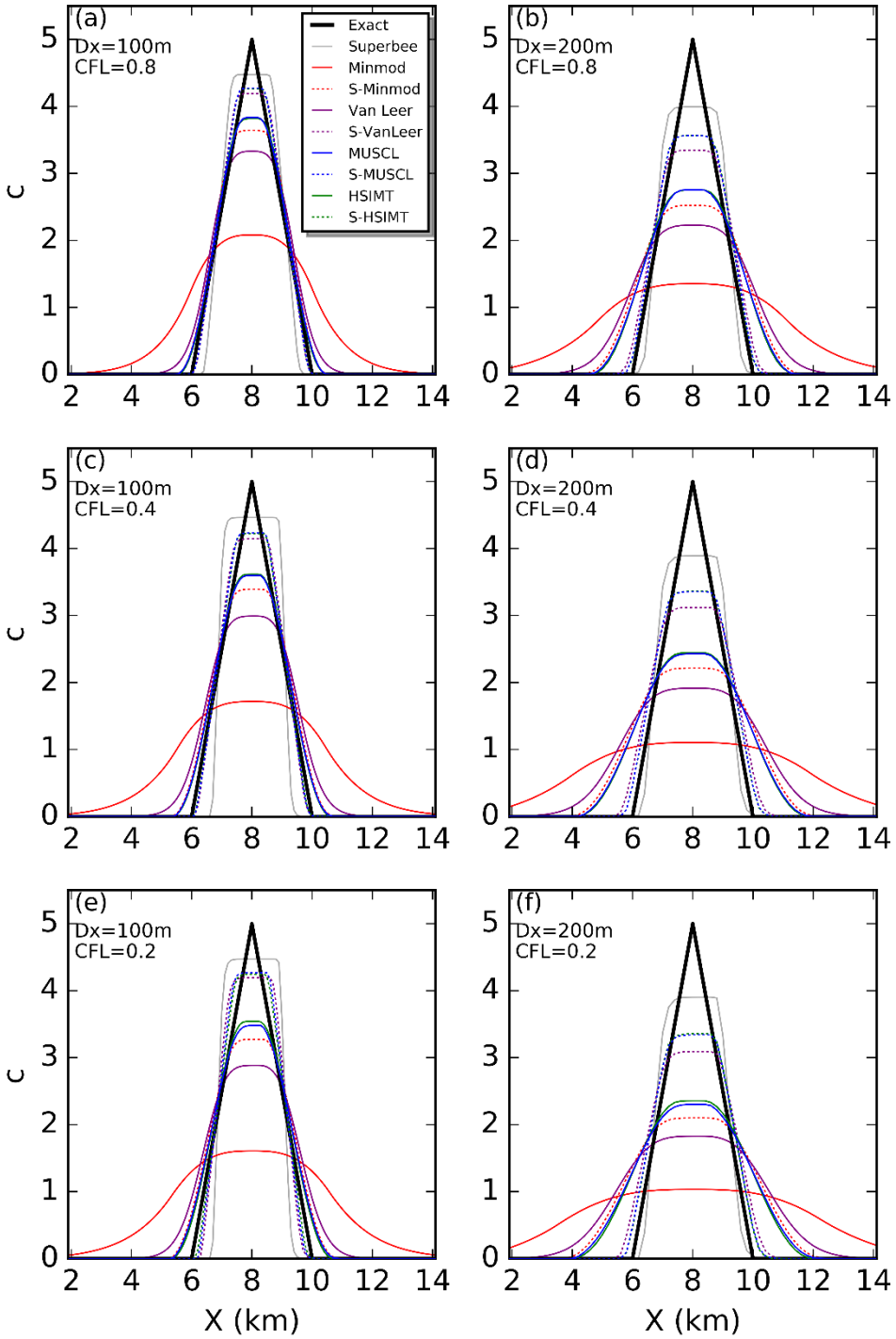

Fig. S2. As in Fig. S1, except for the triangle distribution advection.

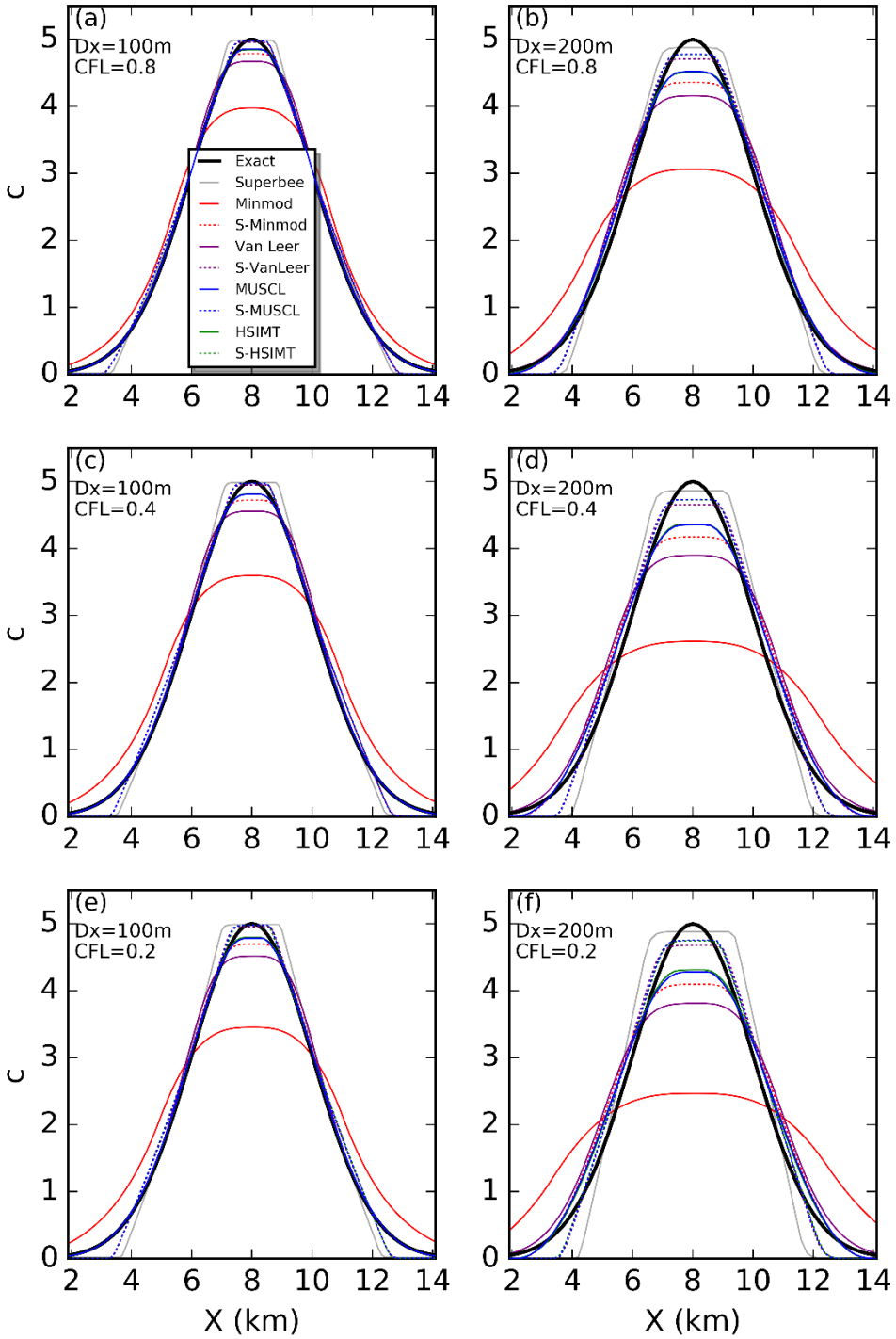

Fig. S3. As in Fig. S1, except for the normal distribution advection.

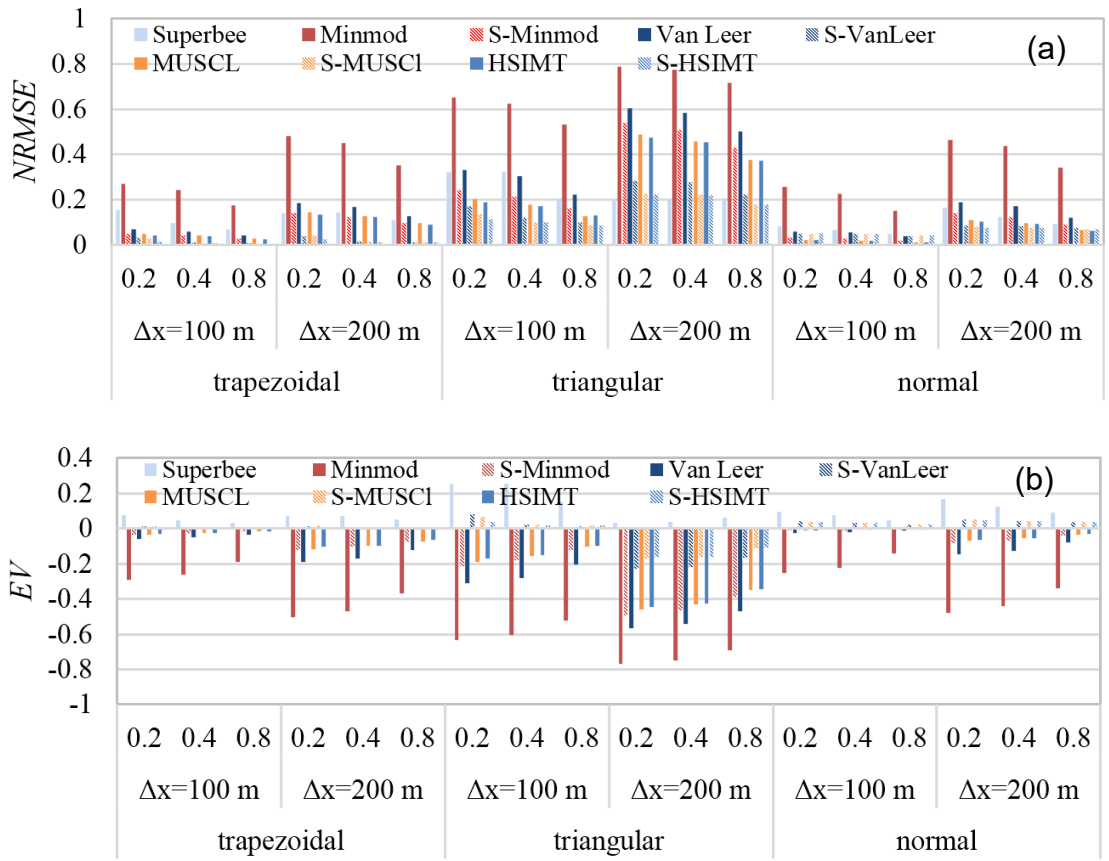

Fig. S4. The *NRMSE*s (a) and *EV*s (b) of the 1D cases for all the tested schemes. The horizontal axis labels (0.2, 0.4, and 0.8) denote the CFL values of each case.

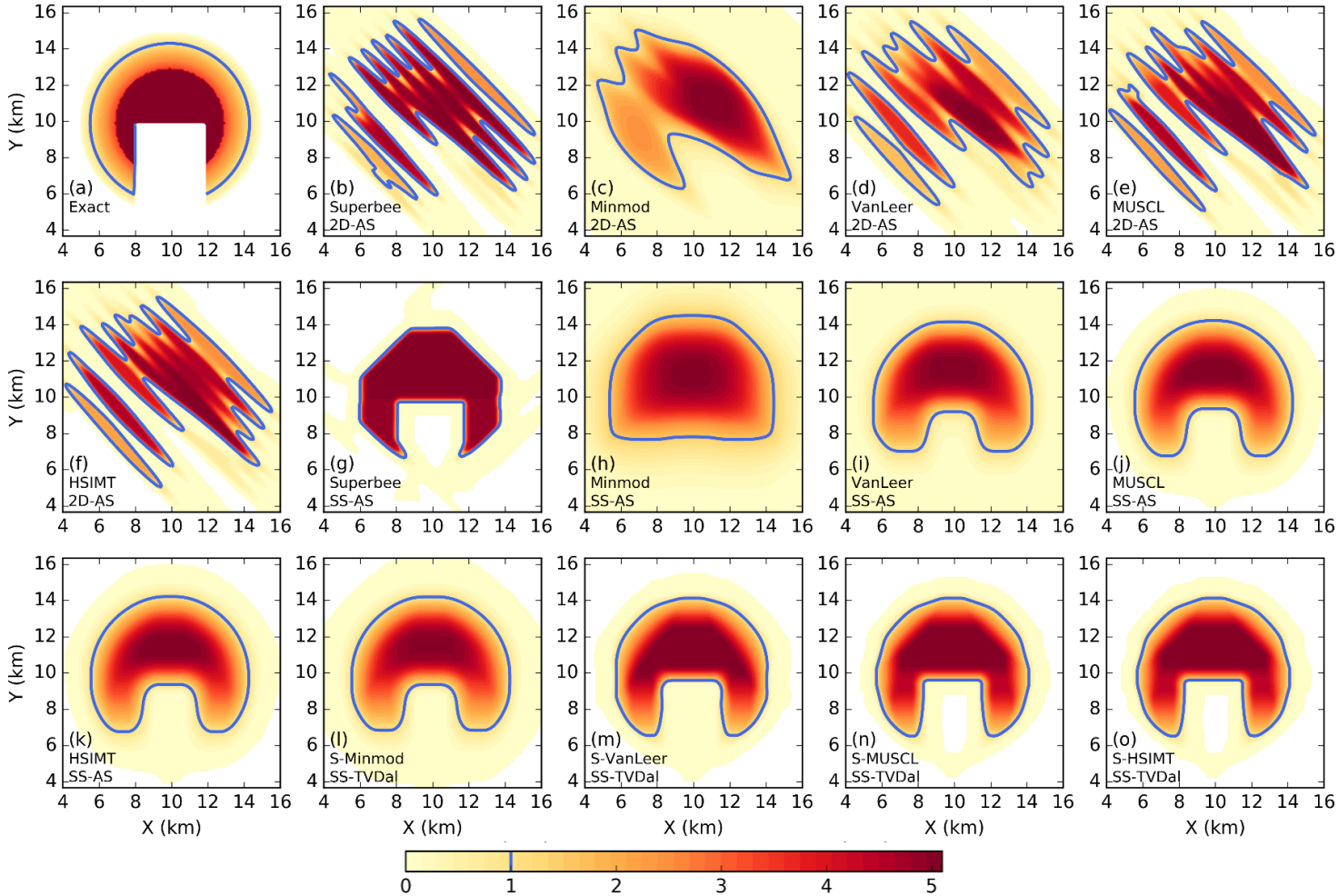

Fig. S5. 2D advection simulation results (the blue line shows the contour line of 1). (a) analytic solution. (b-f) are the results of unsplit schemes (2D-AS). (g-K) are the results TVD with Strang-split method (SS-AS), and (l-o) are the results of TVDal with Strang-split method (SS-TVDal).

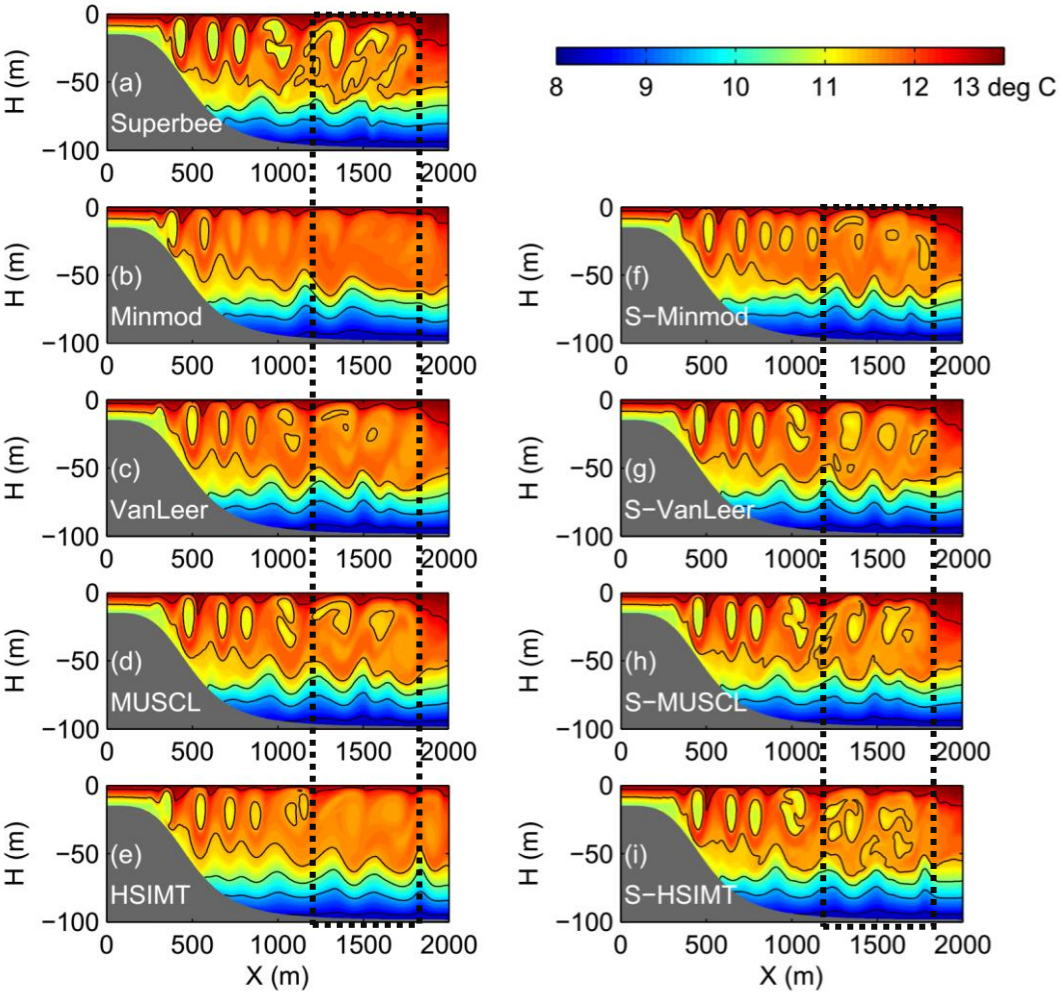

Fig. S6. Snapshots of the temperature distributions at 1/4 of the tidal cycle obtained from the different advection schemes for the lee-wave testcase. From the bottom up, the black lines are the 8.5, 9.5, 10.5, 11.5 and 12.5 °C contours. The black dashed boxes show the region from x=1200 m to 1800 m.

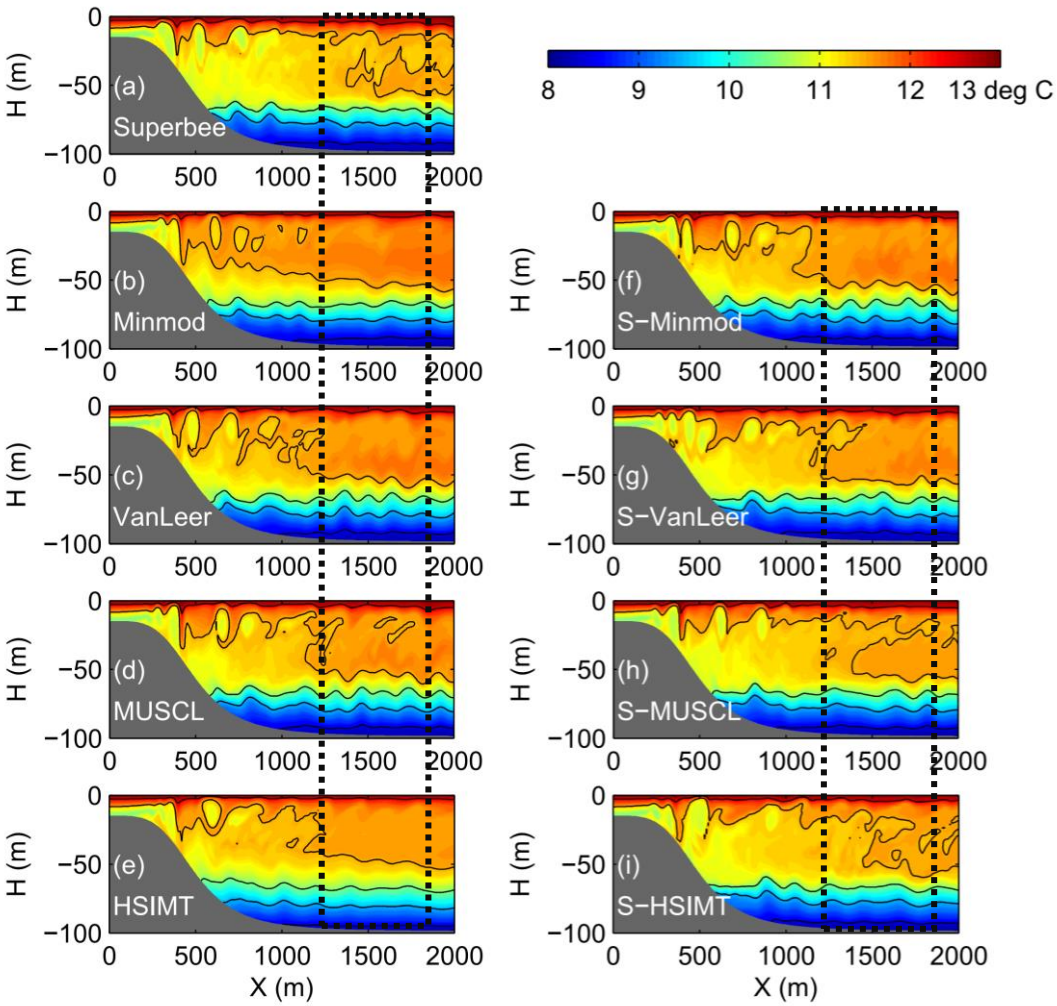

Fig. S7. Snapshots of the temperature distributions at 1/2 of the tidal cycle obtained from the different advection schemes, as shown in Fig. S6.